



Cite this: RSC Adv., 2016, 6, 23599

# Biosorption of $Zn^{2+}$ , $Ni^{2+}$ and $Co^{2+}$ from water samples onto *Yarrowia lipolytica* ISF7 using a response surface methodology, and analyzed by inductively coupled plasma optical emission spectrometry (ICP-OES)

Arash Asfaram,<sup>a</sup> Mehrorang Ghaedi<sup>\*a</sup> and Gholam Reza Ghezelbash<sup>\*b</sup>

A response surface methodology (RSM) based on a central composite design with five variables and five levels was employed to interpret the biosorption efficiency of  $Zn^{2+}$ ,  $Ni^{2+}$  and  $Co^{2+}$  ions onto *Yarrowia lipolytica* ISF7. Independent variables, *viz.* pH, temperature, and  $Zn^{2+}$ ,  $Ni^{2+}$  and  $Co^{2+}$  ion concentrations were transformed into coded values and a quadratic model was built to predict the responses. Analysis of variance (ANOVA) and *t*-test statistics were used to test the significance of the independent variables and their interactions. The predicted maximum biosorption efficiencies (99.65, 99.30 and 98.78% for  $Zn^{2+}$ ,  $Ni^{2+}$  and  $Co^{2+}$  ions, respectively) under the optimum recommended conditions (pH 6.0, 25 °C, 30, 25 and 30 mg L<sup>-1</sup> of  $Zn^{2+}$ ,  $Ni^{2+}$  and  $Co^{2+}$  ions) following 24 h mixing were very close to the experimental values (99.65, 99.30 and 98.78% for  $Zn^{2+}$ ,  $Ni^{2+}$  and  $Co^{2+}$  ions, respectively). The equilibrium equation was extensively investigated and found to be efficiently represented by a Langmuir model with maximum monolayer biosorption capacities of 31.96, 24.40 and 25.77 mg g<sup>-1</sup> for  $Zn^{2+}$ ,  $Ni^{2+}$  and  $Co^{2+}$ , respectively. The biosorption data trend closely followed a pseudo-second-order kinetic model. FTIR and scanning electron microscopy coupled with X-ray energy dispersed analysis (SEM-EDX) provided proof of progress of ion biosorption on the yeast surfaces.

Received 18th December 2015

Accepted 8th February 2016

DOI: 10.1039/c5ra27170c

[www.rsc.org/advances](http://www.rsc.org/advances)

## 1. Introduction

Water pollution caused by heavy metal ions and organic compounds remains a serious problem for the environment and public health.<sup>1–4</sup> Heavy metal ions (antimony, arsenic, beryllium, cadmium, chromium, copper, lead, mercury, nickel, selenium, silver, thallium and zinc) are non-biodegradable, toxic and carcinogenic compound harmful to organisms even at very low concentrations and lead to the generation of hazards and injury to public health.<sup>5–8</sup>

$Ni^{2+}$  ions are a major concern because of their extensive application in developing countries and their potential pollution effects. This metal is released into the environment by many processes such as electroplating, leather tanning, wood preservation, pulp processing, steel manufacturing, plastic pigmentation, mining and metallurgical processes.<sup>9–11</sup> Excess  $Zn^{2+}$  ion intake leads to respiratory problems with breathing rate, volume and frequency of ventilation, coughing, and

a decrease in oxygen uptake efficiency.<sup>12–14</sup>  $Co^{2+}$  ions as used in the manufacture of super alloys, lithium ion batteries, oxidation catalysts and as pigments in paints<sup>15,16</sup> can lead to the discharge of high levels of cobalt contaminated effluents into the aquatic environment, which has encouraged researchers to design and develop effective clean up technologies to remove heavy metals from aquatic media.<sup>17,18</sup>

Conventional heavy metal ion removal protocols *viz.* adsorption, precipitation, ion exchange, biosorption, membrane filtration, electrochemical processes and reverse osmosis have their unique advantages but also suffer from disadvantages such as non-quantitative removal efficiency, high energy consumption and the generation of toxic sludge, which needs proper recycling disposal that is limited from a financial view point.<sup>19–22</sup> Easy to operate and cheap materials that have selective binding with alkaline metals compared to physicochemical processes and that have high efficiency for heavy metal ion biosorption using various waste biomaterials from different parts of world are described below:<sup>23–25</sup> *Aspergillus niger* (for Ni, Co and Zn),<sup>26,27</sup> *Saccharum bengalense* (for Ni and Co),<sup>28,29</sup> brown algae (for Zn and Ni);<sup>30</sup> cross-linked metal-imprinted chitosans with epichlorohydrin (for Zn and Ni);<sup>31</sup> *Chrysanthemum indicum* (for Co);<sup>16</sup> *Sophora japonica* pod powder (for Zn and Ni);<sup>32</sup> *Sargassum glaucescens* nanoparticles (for Zn and Ni);<sup>33</sup> *Hizikia fusiformis* (for Zn,

<sup>a</sup>Chemistry Department, Yasouj University, Yasouj 75918-74831, Iran. E-mail: m\_ghaedi@mail.yu.ac.ir; m\_ghaedi@yahoo.com; Fax: +98 741 2223048; Tel: +98 741 2223048

<sup>b</sup>Biology Department, Faculty of Science, Shahid Chamran University of Ahvaz, 61357-83135, Ahvaz, Iran. E-mail: ghr.ghezelbash@gmail.com; Tel: +98 611 33331045

Ni, Cd and Pb);<sup>34</sup> and *Saccharomyces cerevisiae* (for Zn and Ni) are same good choices for such purposes.<sup>35</sup>

*Yarrowia lipolytica* is non-conventional yeast with significant biological relevance and biotechnological applications. This yeast is a good candidate<sup>36</sup> for biosorption and remediation degradation of different wastes and complicated materials.<sup>37,38</sup> *Yarrowia lipolytica* is able to utilize a variety of renewable carbon sources and the biomass of the yeast has been used as a single cell protein or single cell oil.<sup>39</sup> Our literature survey through most documents did not show any reports nor applications of *Yarrowia lipolytica* to biomass for the simultaneous biosorption of metal ions, while surviving in presence of metal ions like Cr<sup>6+</sup>, Ni<sup>2+</sup>, Co<sup>2+</sup>, Cu<sup>2+</sup>, Cd<sup>2+</sup>, Zn<sup>2+</sup> and Au<sup>2+</sup> that cause stress and accumulate.<sup>40-43</sup> This yeast displays potential for the bioremediation of metal ion polluted environments.

Inductively coupled plasma mass spectrometry (ICP-MS),<sup>44</sup> inductively coupled plasma optical emission spectrometry (ICP-OES),<sup>45-47</sup> flame atomic absorption (FAAS),<sup>48</sup> electrothermal atomic absorption spectrometry (ETAAS),<sup>49</sup> and molecular spectrophotometry and other atomic and molecular conventional instrumental techniques have been applied to quantify metals in many samples. Among the available analytical techniques to quantify the elements present in water samples, inductively coupled plasma optical emission spectrometry (ICP-OES) is a multi-element analysis technique that can lead to the achievement of relatively low detection limits and has a practical linear range that makes possible simultaneous and precise determinations in short times over wide concentration ranges.<sup>50,51</sup>

Optimization of heavy metal ion biosorption efficiencies and their correlation to variables (*i.e.*, pH, temperature and heavy metal concentration) – separately known as a “one factor at a time optimization approach” – is based on maintaining all others at a fixed level. This method is extremely time consuming and expensive for a large number of variables and this limitation can simply be eliminated or lowered by simultaneous and collective optimization using a Central Composite Design (CCD) under a response surface methodology (RSM).<sup>26</sup> The CCD model was based on the statistical evaluation of the following tests: the root-mean-square error (RMSE), bias index and accuracy factor and the lack-of-fit test. The CCD minimizes the number of factor combinations and maintains good precision of the predicted response.<sup>52</sup>

The main objectives of the present study include the following:

- (1) in the present investigation, *Yarrowia lipolytica* ISF7 was isolated from wastewater and subsequently applied for Zn<sup>2+</sup>, Ni<sup>2+</sup> and Co<sup>2+</sup> ion removal from aqueous solution;
- (2) to construct a mathematical equation following statistical optimization to maximize the metal ion sorption efficiency (%) using RSM; and
- (3) to investigate isotherm and kinetic models that describe the biosorption process.

## 2. Materials and methods

### 2.1. Preparation of the biomass

*Yarrowia lipolytica* ISF7 was isolated from wastewater and registered at the NCBI Gene bank with accession number

JX010454.1 and was used laterally for the biosorption of the metal ions under study. *Yarrowia lipolytica* ISF7 was streaked on Yeast–Peptone–Glucose (YPG; 1% yeast extract, 2% peptone, 1% glucose) agar and incubated overnight at 30 °C. Then a single colony was inoculated into a 100 mL Erlenmeyer flask containing 25 mL of YPG broth (pH: 7.0) incubated on a shaker (160 rpm) for 24 h at 30 °C.

### 2.2. Metals and chemicals

The yeast extract, peptone, glucose, agar and Zn(NO<sub>3</sub>)<sub>2</sub>·6H<sub>2</sub>O, Ni(NO<sub>3</sub>)<sub>2</sub>·6H<sub>2</sub>O and Co(NO<sub>3</sub>)<sub>2</sub>·6H<sub>2</sub>O used in all the experiments were obtained from Sigma-Aldrich. NaOH and HCl with the highest purity available were purchased from Merck (Darmstadt, Germany). Several stock solutions of Zn, Ni and Co in deionized water were prepared, ranging from 10 to 100 mg L<sup>-1</sup>, from their water-soluble metallic salts (Zn(NO<sub>3</sub>)<sub>2</sub>·6H<sub>2</sub>O, Ni(NO<sub>3</sub>)<sub>2</sub>·6H<sub>2</sub>O and Co(NO<sub>3</sub>)<sub>2</sub>·6H<sub>2</sub>O) and stored in 500 mL volumetric flasks for posterior metal ion biosorption experiments.

### 2.3. Instrumentation

Fourier transform infrared spectroscopy (FT-IR) studies were investigated using 1 mg samples in strained cells before and after metal ion biosorption, respectively. Infrared spectra were recorded using a Perkin-Elmer spectrometer, RX-IIFTIR, USA) in the range of 4000–300 cm<sup>-1</sup>. Inductively coupled plasma optical emission spectrometry (ICP-OES, Optima 8300, Perkin Elmer) was used for the determination of analytes with transitions at 213.854 nm (4s), 231.604 nm (5s) and 228.613 nm (4s), *i.e.* Zn<sup>2+</sup>, Ni<sup>2+</sup> and Co<sup>2+</sup>, respectively. The spectroscopic technique EDAX, which uses a scanning electron microscope (Oxford INCA II energy solid state detector), was used to characterize the material used, before and after equilibration with the metal ions. The pH measurements were carried out using a digital pH meter (Ino Lab pH 730, Germany). A HERMLE bench centrifuge (2206 A, Germany) was used to accelerate the phase separation. The samples were agitated in an incubator shaker (Labcon, FSIM-SPO16, United States) at 160 rpm. Response surface analysis was performed with the STATISTICA software version 10.0 (Stat Soft Inc., Tulsa, USA). The significance of all the terms in the polynomial equation were analyzed statistically by computing the *F*-value at a probability (*p*) of 0.05.

### 2.4. Batch biosorption studies

Following growth on YPG agar, a single colony was inoculated into a 100 mL Erlenmeyer flask containing 25 mL of YGC broth together with 10–40 mg L<sup>-1</sup> of Zn<sup>2+</sup>, Ni<sup>2+</sup> and Co<sup>2+</sup> ions. The flasks were agitated in a shaker at 160 rpm over various temperatures and times and biosorption equilibrium was reached after 24 h. The required pH value of the solutions was adjusted with HCl and/or NaOH solutions. In the batch biosorption experiments, samples were taken at given time intervals and were centrifuged at 3000 rpm for 10 min. Subsequently the supernatant part was analyzed for the non-sorbed metal ions being studied by inductively coupled plasma optical emission spectrometry (ICP-OES). The sediment phase (yeast)

was again centrifuged and the remaining biomass was dried at 65 °C for 24 h. Biosorption isotherm studies were examined over 10–100 mg L<sup>-1</sup> of the target compounds. The biosorption capacity ( $q_e$ ), *i.e.* the amount of metal ion (mg) biosorbed per gram of the biomass, and the efficiency of biosorption ( $R\%$ ) were calculated using eqn (1) and (2), respectively:

$$q_{\text{eq}} = \frac{C_i - C_f}{X_0} \quad (1)$$

$$\text{Biosorption percentage}(R\%) = \frac{C_i - C_f}{C_i} \times 100\% \quad (2)$$

where  $C_i$  and  $C_f$  are the metal ion concentrations at the initial time and at equilibrium (mg L<sup>-1</sup>), and  $X_0$  is the biosorbent concentration (g L<sup>-1</sup>). Kinetic studies were used to investigate the effect of contact time and initial concentration to subsequently determine the kinetic parameters. All the investigations were carried out in triplicate to avoid any discrepancy in the experimental results, enhance reproducibility and lower the relative standard deviations to  $\pm 0.5\%$  and  $\pm 2.3\%$ , respectively.

The applicability of each model was judged by a chi-square ( $\chi^2$ ) test and the coefficient of determination ( $R^2$ ) as criteria to obtain the best isotherm and kinetic models for describing the

**Table 1** Experimental factors and levels in the central composite design for ion biosorption<sup>c</sup>

Factors	Units	Levels			$\alpha = 2$								
		Low (-1)	Central (0)	High (+1)	$-\alpha$	$+\alpha$							
$X_1$ : pH	—	5.0	6.0	7.0	4.0	8.0							
$X_2$ : temperature	°C	25	30	35	20	40							
$X_3$ : Zn <sup>2+</sup> concentration	mg L <sup>-1</sup>	25	30	35	20	40							
$X_4$ : Ni <sup>2+</sup> concentration	mg L <sup>-1</sup>	15	20	25	10	30							
$X_5$ : Co <sup>2+</sup> concentration	mg L <sup>-1</sup>	15	20	25	10	30							
Factors					$R\%_{\text{Zn}^{2+}}$								
Run	$X_1$	$X_2$	$X_3$	$X_4$	$X_5$	Exp. <sup>a</sup>	Pred. <sup>b</sup>	$R\%_{\text{Ni}^{2+}}$	Exp. <sup>a</sup>	Pred. <sup>b</sup>	$R\%_{\text{Co}^{2+}}$	Exp. <sup>a</sup>	Pred. <sup>b</sup>
1 (F)	5.0	25	25	15	25	89.34	89.09	91.56	90.88	84.71	84.39		
2 (F)	7.0	25	25	15	15	88.90	88.54	95.68	95.01	97.26	96.75		
3 (F)	5.0	35	25	15	15	85.63	85.34	91.21	90.76	91.84	91.53		
4 (F)	7.0	35	25	15	25	90.64	90.39	95.65	95.19	92.82	92.28		
5 (F)	5.0	25	35	15	15	90.45	89.82	93.67	93.20	91.92	91.58		
6 (F)	7.0	25	35	15	25	94.76	94.16	97.89	97.41	89.28	88.72		
7 (F)	5.0	35	35	15	25	84.65	84.12	88.34	88.09	86.84	86.48		
8 (F)	7.0	35	35	15	15	86.73	86.10	90.34	90.10	92.73	92.18		
9 (F)	5.0	25	25	25	15	92.66	92.24	90.23	89.83	90.07	89.82		
10 (F)	7.0	25	25	25	25	98.77	98.38	96.64	96.23	95.06	94.59		
11 (F)	5.0	35	25	25	25	88.34	88.02	83.43	83.25	77.44	77.17		
12 (F)	7.0	35	25	25	15	85.67	85.24	94.78	94.61	97.48	97.02		
13 (F)	5.0	25	35	25	25	81.67	81.01	86.34	86.14	91.71	91.42		
14 (F)	7.0	25	35	25	15	90.23	89.46	91.23	91.04	95.39	94.90		
15 (F)	5.0	35	35	25	15	85.98	85.28	87.80	87.83	85.34	85.05		
16 (F)	7.0	35	35	25	25	90.23	89.57	91.21	91.23	90.61	90.10		
17 (A)	4.0	30	30	20	20	58.76	59.67	61.00	61.66	58.01	58.41		
18 (A)	8.0	30	30	20	20	65.34	66.40	71.23	71.88	69.45	70.68		
19 (A)	6.0	20	30	20	20	97.35	98.41	96.89	97.99	96.15	96.95		
20 (A)	6.0	40	30	20	20	90.34	91.26	93.12	93.32	91.02	91.86		
21 (A)	6.0	30	20	20	20	97.89	98.26	97.98	99.04	97.84	98.60		
22 (A)	6.0	30	40	20	20	92.21	93.82	96.12	96.36	96.94	97.82		
23 (A)	6.0	30	30	10	20	96.78	97.56	99.89	101.09	95.93	96.86		
24 (A)	6.0	30	30	30	20	96.78	97.97	95.87	95.97	95.20	95.90		
25 (A)	6.0	30	30	20	10	94.88	96.01	97.90	98.53	99.89	100.67		
26 (A)	6.0	30	30	20	30	98.35	99.19	96.87	97.54	91.40	92.25		
27 (C)	6.0	30	30	20	20	94.76	95.09	90.56	91.49	89.84	89.01		
28 (C)	6.0	30	30	20	20	95.64	95.09	92.62	91.49	88.41	89.01		
29 (C)	6.0	30	30	20	20	96.89	95.09	91.28	91.49	89.45	89.01		
30 (C)	6.0	30	30	20	20	95.34	95.09	92.01	91.49	90.29	89.01		
31 (C)	6.0	30	30	20	20	94.67	95.09	91.88	91.49	88.77	89.01		
32 (C)	6.0	30	30	20	20	95.23	95.09	91.90	91.49	88.93	89.01		

<sup>a</sup> Experimental values of response. <sup>b</sup> Predicted values of response by the proposed RSM model. <sup>c</sup> (C): center point. (F): factorial point. (A): axial point.

experimental equilibrium data in non-linear regression analysis.<sup>53</sup>

The following non-linear chi-square test ( $\chi^2$ )<sup>54</sup> was carried out on the best-fitted isotherm:

$$\chi^2 = \sum \frac{(q_{e,\text{exp}} - q_{e,\text{cal}})^2}{q_{e,\text{cal}}} \quad (3)$$

where  $q_{e,\text{exp}}$  and  $q_{e,\text{cal}}$  are the experimental and calculated biosorption capacities. A small value of  $\chi^2$  indicates that the data obtained from the model is consistent with the experimental values.

## 2.5. Statistical analysis

The optimum conditions for maximum  $\text{Zn}^{2+}$ ,  $\text{Ni}^{2+}$  and  $\text{Co}^{2+}$  ion biosorption by yeast were determined by means of a five factor test which selected at five levels namely lowest, low, medium, high and highest, coded as  $-\alpha$ ,  $-1$ ,  $0$ ,  $+1$  and  $+\alpha$  in a central composite experimental design (CCD) combined with a response surface methodology. Five critical parameters of concern for biosorption, pH ( $X_1$ ), temperature ( $X_2$ ), and  $\text{Zn}^{2+}$ ,  $\text{Ni}^{2+}$  and  $\text{Co}^{2+}$  concentration ( $X_3$ ,  $X_4$  and  $X_5$ , respectively), were selected as independent variables based on preliminary experiments while removal biosorption % ( $Y$ ) was the dependent variable (response). The experimental range and levels of independent variables for metal ion biosorption are given in Table 1 and subsequently were analyzed using STATISTICA 10.0, following which the regression model was proposed. In the optimization process, the responses can be simply related to the chosen factors by linear or quadratic models. A quadratic model, which also includes the linear model, is given below as eqn (4):<sup>55</sup>

$$y = \beta_0 + \sum_{i=1}^k \beta_i x_i + \sum_{i=1}^k \sum_{j=1}^k \beta_{ij} x_i x_j + \sum_{i=1}^k \beta_{ii} x_i^2 + \varepsilon \quad (4)$$

where  $y$  denotes the response;  $k$  is the number of variables;  $x_i$  symbolizes the independent variables;  $\varepsilon$  is the residual associated with the experiments;  $\beta_0$  is the constant coefficient; and  $\beta_i$ ,  $\beta_{ii}$ , and  $\beta_{ij}$  represent the coefficients of the linear, quadratic, and interaction parameters.<sup>56</sup>

A total of 32 experiments performed in randomized order were used to construct diagnostic checking tests provided by analysis of variance (ANOVA). The properties of the fit polynomial model are represented by the coefficient of determination  $R^2$ . The  $R^2$  values measure how variability in the observed response values can be clarified by experimental factors and their interactions. These analyses are performed by Fisher's 'F'-test and  $P$ -value (probability). Based on the experimental data, the levels of the five main parameters investigated in this study are presented in Table 1.

## 3. Results and discussion

### 3.1. Effect of contact time on biosorption efficiency

The influence of contact time on the batch biosorption of 10 mg L<sup>-1</sup> of the studied analytes at 25 °C, pH 5.5 and different time intervals (6–48 h) are shown in Fig. 1. It is obvious that rising

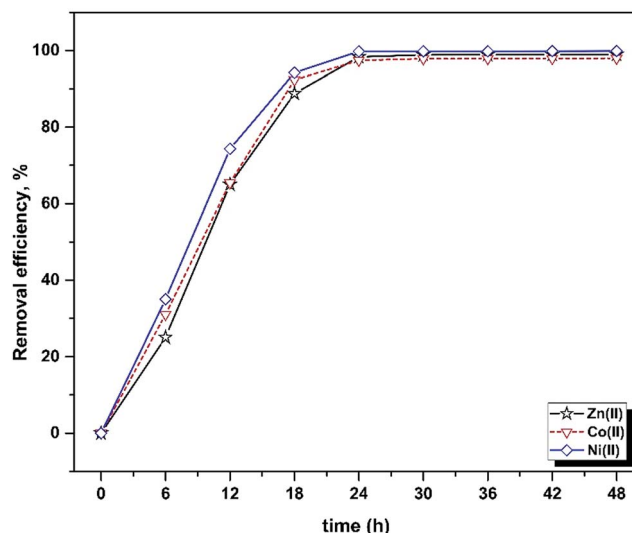


Fig. 1 Influence of contact time on the removal efficiency of *Yarrowia lipolytica* ISF7 (ion concentration = 10 mg L<sup>-1</sup>, 25 °C, pH = 5.5).

contact time causes a significant increase in the biosorption percentage, which was very rapid at the beginning stage but was found to reach plateau values within 24 h. The trends and magnitudes of their binding to biomass reveal the contribution and participation of the functional groups of the biomass to complex metal ions. Biosorption occurs in two stages: an initial rapid uptake, where the surface of the cell wall components attract metal ions, and a subsequent slow uptake due to their membrane transport. The cell surfaces of many microorganisms consist of polysaccharides, proteins and lipids containing several functional groups which are capable of binding metal ions.<sup>57,58</sup> The biosorption rate depends on the structural properties of the sorbate and biosorbent (e.g. protein and carbohydrate composition), surface charge density, topography, surface area, initial concentration of metal ions and the existence of other ions.<sup>59,60</sup>

### 3.2. Fitting the process models

CCD was adopted to study the correlation of the target compound biosorption efficiency with variables like pH, temperature, and  $\text{Zn}^{2+}$ ,  $\text{Ni}^{2+}$  and  $\text{Co}^{2+}$  ion concentrations. A quadratic model was selected for developing the mathematical relationship between the responses and the five operating variables. The present CCD consists of 16 standard factorial runs, a star configuration ( $\alpha = \pm 2$ ) based on 10 experiments and six replicates at the center point, which were finally used to determine the experimental error. The predicted and actual responses (Table 1) reveal that the maximum metal ion biosorptions were 99.65, 99.30 and 98.78% for  $\text{Zn}^{2+}$ ,  $\text{Ni}^{2+}$  and  $\text{Co}^{2+}$ , respectively. Following polynomial regression models correlation of the biosorption of each ion to the corresponding coded values ( $X_1$ ,  $X_2$ ,  $X_3$ ,  $X_4$  and  $X_5$ ) of the five different process variables (pH, temperature,  $\text{Zn}^{2+}$ ,  $\text{Ni}^{2+}$  and  $\text{Co}^{2+}$  ions concentration), finally the best fitted model was obtained as:

$$\begin{aligned} R\%_{\text{Zn}^{2+}} = & -121 + 87.60X_1 - 0.70X_2 - 0.60X_3 - 2.55X_5 \\ & - 0.42X_1X_5 - 0.05X_3X_4 - 0.041X_3X_5 - 0.008X_4X_5 \\ & - 8.1X_1^2 + 0.03X_4^2 + 0.03X_5^2 \end{aligned} \quad (5)$$

$$\begin{aligned} R\%_{\text{Ni}^{2+}} = & 31.4 + 72.1X_1 - 2.62X_2 - 2.8X_3 - 3.58X_4 \\ & - 0.12X_1X_3 + 0.2X_1X_4 + 0.3X_1X_5 - 0.012X_3X_4 \\ & - 6.2X_1^2 + 0.042X_2^2 + 0.06X_3^2 + 0.07X_4^2 + 0.07X_5^2 \end{aligned} \quad (6)$$

$$\begin{aligned} R\%_{\text{Co}^{2+}} = & 56.7 + 76.1X_1 - 2.71X_2 - 5.03X_5 \\ & + 0.17X_1X_2 - 0.33X_1X_3 + 0.22X_1X_4 - 0.07X_2X_4 \\ & + 0.05X_3X_5 - 6.12X_1^2 + 0.054X_2^2 + 0.092X_3^2 \\ & + 0.074X_4^2 + 0.075X_5^2 \end{aligned} \quad (7)$$

The ANOVA results of this quadratic model (Table 2) could be used to navigate the design space. The significance of coefficients was determined from *F* and *P* values. The application of ANOVA is found to be the most reliable way for the evaluation of quality of the fitted model.<sup>26</sup> By using ANOVA, the variation can be compared among independent variables with respect to response.

Values of Prob > *F* less than 0.0500 indicate that the model terms are significant for biosorption of  $\text{Zn}^{2+}$ ,  $\text{Ni}^{2+}$  and  $\text{Co}^{2+}$  ions. The non-significant lack-of-fit (more than 0.05) supports the validity of the present quadratic model for the present study. The non-significant lack-of-fit shows the goodness of the

equation for the prediction of experimental data. The predicted and adjusted *R*<sup>2</sup> values of 0.8427 and 0.9772 for  $\text{Zn}^{2+}$  ion, 0.8911 and 0.9835 for  $\text{Ni}^{2+}$  ion and 0.8881 and 0.9833 for  $\text{Co}^{2+}$  ion has reasonable agreement with the desirable *R*<sup>2</sup> value of 1.0 and indicates the better fitness of the model to the experimental data (see Table 3).

The residual variation is measured using the coefficient of variance (CV) relative to the size of the mean. A very low value of

**Table 3** Quality of the quadratic model based on *R*<sup>2</sup> and the standard deviation for the biosorption of ions onto *Yarrowia lipolytica* ISF7

Quality of quadratic model based on <i>R</i> <sup>2</sup> and the standard deviation							
Response	SD <sup>a</sup>	<i>R</i> <sup>2b</sup>	Adj- <i>R</i> <sup>2c</sup>	Pred- <i>R</i> <sup>2d</sup>	Mean	CV% <sup>e</sup>	AP <sup>f</sup>
$\text{Zn}^{2+}$	1.3120	0.9919	0.9772	0.8427	90.180	1.455	37.170
$\text{Ni}^{2+}$	0.9870	0.9942	0.9835	0.8911	91.350	1.081	49.300
$\text{Co}^{2+}$	1.0820	0.9941	0.9833	0.8881	89.940	1.203	48.220

<sup>a</sup> Standard deviation: square root of the pure (experimental) error.

<sup>b</sup> Coefficient of determination. <sup>c</sup> Adjusted coefficient of determination.

<sup>d</sup> Predicted coefficient of determination. <sup>e</sup> Coefficient of variation, the standard deviation as a percentage of the mean. <sup>f</sup> Adequate precision: compares the range of predicted values at design points to the average prediction error.

**Table 2** Analysis of variance (ANOVA) for the ion biosorption onto *Yarrowia lipolytica* ISF7<sup>d</sup>

Source of variation	Df <sup>a</sup>	Zn <sup>2+</sup>			Ni <sup>2+</sup>			Co <sup>2+</sup>					
		SS <sup>b</sup>	MS <sup>c</sup>	F-Value	P-Value	SS	MS	F-Value	P-Value	SS	MS	F-Value	P-Value
Model	20	2324.9	116.24	67.497	<0.0001	1822.6	91.128	93.498	<0.0001	2155.8	107.8	92.097	<0.0001
$X_1$	1	67.906	67.906	39.430	<0.0001	156.54	156.54	160.611	<0.0001	225.95	225.95	193.056	<0.0001
$X_2$	1	76.791	76.791	44.589	<0.0001	32.713	32.713	33.564	0.000120	38.913	38.913	33.248	0.000125
$X_3$	1	29.504	29.504	17.131	0.00168	10.774	10.774	11.054	0.006774	0.905	0.905	0.773	0.3981
$X_4$	1	0.250	0.250	0.145	0.7104	39.322	39.322	40.344	<0.0001	1.382	1.382	1.181	0.3004
$X_5$	1	15.185	15.185	8.817	0.01276	1.470	1.470	1.508	0.2450	106.43	106.43	90.934	<0.0001
$X_1X_2$	1	6.089	6.089	3.535	0.08680	0.152	0.152	0.156	0.7004	11.560	11.560	9.877	0.009362
$X_1X_3$	1	7.826	7.826	4.544	0.05641	8.702	8.702	8.929	0.01234	43.428	43.428	37.106	<0.0001
$X_1X_4$	1	1.749	1.749	1.016	0.3352	7.952	7.952	8.159	0.01562	18.490	18.490	15.798	0.002179
$X_1X_5$	1	70.518	70.518	40.946	<0.0001	31.922	31.922	32.753	0.000134	0.714	0.714	0.610	0.4512
$X_2X_3$	1	6.089	6.089	3.535	0.08680	0.360	0.360	0.369	0.5557	1.729	1.729	1.477	0.2496
$X_2X_4$	1	0.452	0.452	0.263	0.6185	2.280	2.280	2.339	0.1544	31.416	31.416	26.842	0.000303
$X_2X_5$	1	3.563	3.563	2.069	0.1782	3.168	3.168	3.251	0.09882	2.103	2.103	1.796	0.2072
$X_3X_4$	1	23.547	23.547	13.672	0.00352	1.346	1.346	1.381	0.2648	4.906	4.906	4.192	0.06526
$X_3X_5$	1	16.626	16.626	9.654	0.00998	1.796	1.796	1.842	0.2019	24.206	24.206	20.682	0.000833
$X_4X_5$	1	0.644	0.644	0.374	0.5533	5.018	5.018	5.148	0.04439	2.756	2.756	2.354	0.1532
$X_1^2$	1	1883.8	1883.8	1093.8	<0.0001	1120.7	1120.7	1149.84	<0.0001	1097.0	1097.0	937.331	<0.0001
$X_2^2$	1	0.124	0.124	0.072	0.7938	31.792	31.792	32.619	0.000134	53.321	53.321	45.559	<0.0001
$X_3^2$	1	1.639	1.639	0.952	0.3503	70.684	70.684	72.522	<0.0001	155.11	155.11	132.524	<0.0001
$X_4^2$	1	13.123	13.123	7.620	0.01854	90.844	90.844	93.207	<0.0001	99.662	99.662	85.153	<0.0001
$X_5^2$	1	11.554	11.554	6.709	0.02513	78.517	78.517	80.559	<0.0001	101.84	101.84	87.010	<0.0001
Residual	11	18.944	1.722			10.721	0.975			12.874	1.170		
Lack-of-fit	6	15.694	2.616	4.024	0.07404	8.231	1.372	2.754	0.1430	10.366	1.728	3.444	0.09800
Pure error	5	3.250	0.650			2.490	0.498			2.508	0.502		
Cor total	31	2343.8				1833.3				2168.7			

<sup>a</sup> Degree of freedom:  $N - 1$ . <sup>b</sup> Sum of square: sums of squares, sum of the squared differences between the average values and the overall mean.

<sup>c</sup> Mean of square: sum of squares divided by Df. <sup>d</sup> *F*-Value: test for comparing term variance with residual (error) variance. Prob > *F*: probability of seeing the observed *F*-value if the null hypothesis is true. Residual: consists of terms used to estimate the experimental error. Lack-of-fit: variation of the data around the fitted model. Pure error: variation in the response in replicated design points. Cor total: totals of all information corrected for the mean.

the CV (<1.4%) implies sufficient precision and reliability of the experimental results. "Adequate Precision" measures the signal to noise ratio, and a ratio greater than 4.0 is desirable. The "Adequate Precision" ratio of this model (>37.00) is far greater than 4.0 which indicates the presence of an adequate signal corresponding to the model.<sup>61</sup>

Fig. 2a shows the correlation between the predicted and experimental values for prediction of the target compound's biosorption and their closeness to each other.

A high value parameter estimate for the variables  $X_1$  and  $X_2$  indicates a high level of significance and interaction on the biosorption process. The variable  $X_1$  (pH) has a positive relation to the studied metal ions' biosorption, whereas  $X_2$  (temperature) shows a negative relationship.

The residual plot for the predicted and experimental values and case number (Fig. 3c and d) reveals that the residual values are uniformly distributed and also suggests that real data are well fitted by eqn (5)–(7), and that it has good agreement with experimental data.

### 3.3. Interactive effects of two variables

The response surface and counter plots for the  $\text{Ni}^{2+}$  ion biosorption efficiency of *Yarrowia lipolytica* ISF7 (Fig. 3a) show the effect of temperature and initial pH on biosorption efficiency. The initial pH and temperature are the most important parameters affecting the biosorption (Fig. 3a) and the maximum efficiency was obtained at pH 6.0 and 25 °C. The  $\text{Ni}^{2+}$  ion biosorption efficiency has a positive relation with a pH up to 6.0 though increased values are associated with a decrease in efficiency.

The surface plot (Fig. 3b) confirms the contribution of the interaction between pH and initial  $\text{Zn}^{2+}$  ion concentration on  $\text{Zn}^{2+}$  ion removal efficiency and the results presented in Fig. 3b shows that the maximum removal efficiency of 98% was achieved at pH of 6.0 and 40 mg L<sup>-1</sup>  $\text{Zn}^{2+}$  ions. This result is due to the influence of pH on the sorption.

### 3.4. Optimization based on desirability functions

In this study, multi-response optimizations by the desirability function of the response surface methodology were implemented to find optimal cutting parameters to determine the maximum biosorption in the least time. First, each response is converted into an individual desirability function that varies over the range from 0 to 1. The unit value indicates the maximum desirable response while a zero value means one or more responses are outside the acceptable region.<sup>62</sup> Finally, the individual desirability functions are combined to provide a measure of the composite desirability of the multi-response system. For multi-response optimization (Table 4), the optimum conditions were pH (6.0), temperature (25 °C) and  $\text{Zn}^{2+}$ ,  $\text{Ni}^{2+}$  and  $\text{Co}^{2+}$  ion concentrations were 30, 25 and 30 mg L<sup>-1</sup>, leading to the achievement of biosorption efficiency responses of 99.65, 99.30 and 98.78%, which are in close agreement with the predicted values of 100.18, 99.63 and 99.43%. Comparing the experimental and predicted responses, it is evident that the biosorption efficiencies are in reasonable

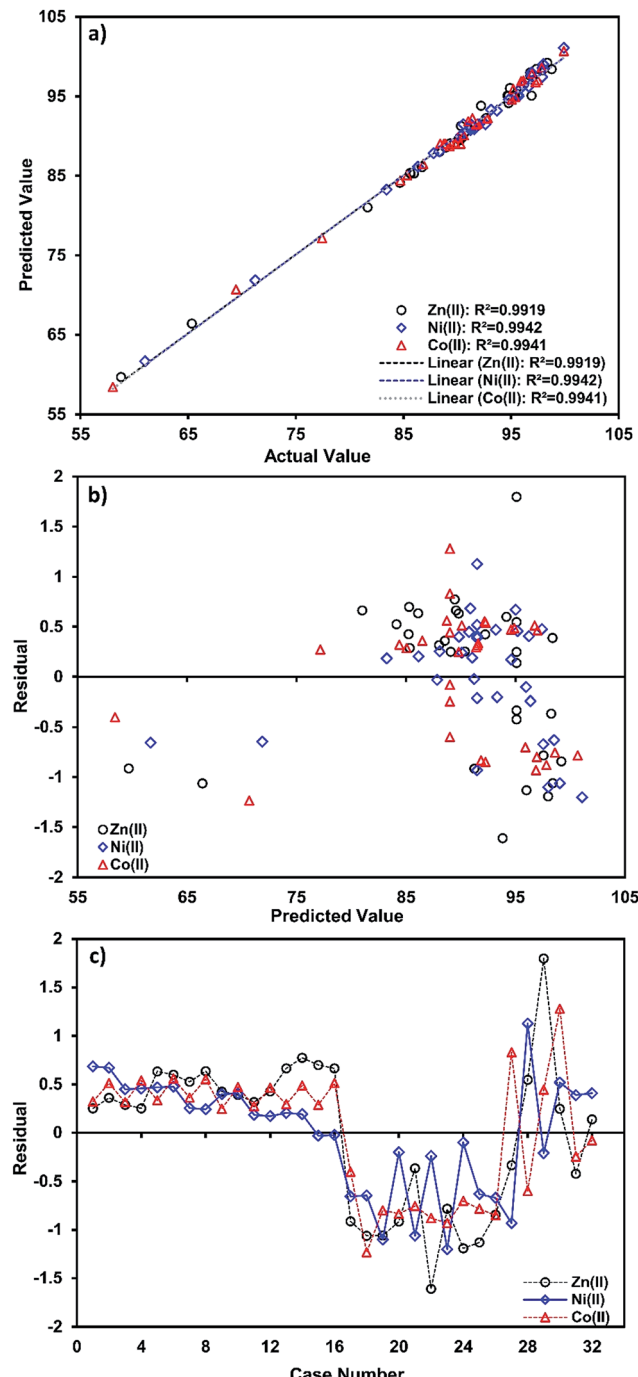


Fig. 2 (a) Correlation of predicted and actual values, (b) the studentized residuals and predicted response plot, and (c) studentized residuals and case number value for ion biosorption.

agreement with the predicted responses, Table 4. A maximum of a 2.5% deviation between the model predictions and experimental average results occurs for  $\text{Zn}^{2+}$ ,  $\text{Ni}^{2+}$  and  $\text{Co}^{2+}$  ions.

### 3.5. Biosorption isotherm model analysis

The equilibrium isotherm is crucial to understand the interaction between sorbate and biosorbent. The data obtained from

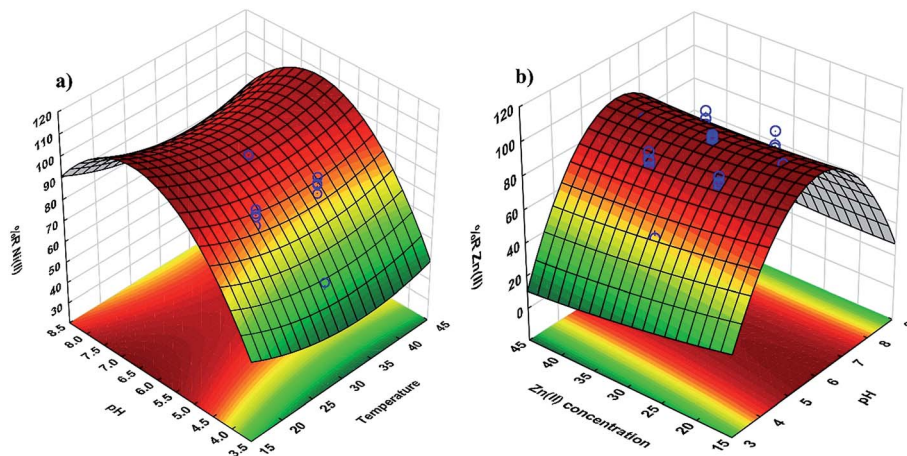


Fig. 3 3D surface mapping plot for the multiple effects of (a) pH and temperature and (b) pH and  $Zn^{2+}$  concentration.

Table 4 Optimum conditions and desirability options for the biosorption of ions onto *Yarrowia lipolytica* ISF7

Exp.	Optimum conditions					Biosorption efficiency (R%)			
	$X_1$	$X_2$	$X_3$	$X_4$	$X_5$	Response	Experimental	Predicted	Desirability
1	6.0	25	30	25	30	$Zn^{2+}$	$99.65 \pm 1.38$	100.18	0.9967
2	6.0	25	30	25	30				
3	6.0	25	30	25	30	$Ni^{2+}$	$99.30 \pm 1.65$	99.62	0.9967
4	6.0	25	30	25	30				
5	6.0	25	30	25	30	$Co^{2+}$	$98.78 \pm 2.11$	99.43	0.9967
6	6.0	25	30	25	30				

the batch experiments were applied to some commonly used isotherm models: Langmuir, Freundlich, Temkin and Dubinin-

Radushkevich. The equations and linearized forms of these isotherm models are given in Table 5.

Table 5 Isotherm constant parameters and correlation coefficients calculated for the biosorption of ions onto *Yarrowia lipolytica* ISF7 in the single component system

Isotherms	Linear expressions	Plot	Parameters	Parameters	$Zn^{2+}$	$Ni^{2+}$	$Co^{2+}$
Langmuir	$1/q_e = 1/(K_L Q_{\max} C_e) + 1/Q_{\max}$	$C_e/q_e$ vs. $C_e$	$Q_{\max} = (\text{slope})^{-1}$ $K_L = \text{slope}/\text{intercept}$	$Q_{\max}$ (mg g <sup>-1</sup> ) $K_L$ (L mg <sup>-1</sup> ) $R^2$	31.96 2.376 0.9962	24.40 0.9995 0.9959	25.77 0.8928 0.9952
Freundlich	$\ln q_e = \ln K_F + (1/n)\ln C_e$	$\log q_e$ vs. $\log C_e$	$n = (\text{slope})^{-1}$ $K_F = \exp(\text{intercept})$	$R_L$ $\chi^2$	0.0042- 0.0404 0.0023	0.0099- 0.0910 0.0019	0.0111- 0.1010 0.0026
Temkin	$q_e = B_1 \ln K_T + B_1 \ln C_e$	$q_e$ vs. $\ln C_e$	$B_1 = (\text{slope})$ $K_T = \exp(\text{intercept}/\text{slope})$	$n$ $K_F$ (L mg <sup>-1</sup> ) $R^2$ $\chi^2$	4.548 3.381 0.9018 4.8620	4.943 2.968 0.8814 6.7023	5.160 3.053 0.8993 6.3240
Dubinin- Radushkevich	$\ln q_e = \ln Q_s - \beta \varepsilon^2$	$\ln q_e$ vs. $\varepsilon^2$	$Q_s = \exp(\text{intercept})$ $\beta = -\text{slope}$ $E = (1/2\beta)^{0.5}$	$Q_s$ (mg g <sup>-1</sup> ) $\beta \times 10^{-8}$ $E$ (kJ mol <sup>-1</sup> ) $R^2$ $\chi^2$	153.66 2.3 4.663 0.8775 6.6231	177.78 2.8 4.226 0.8871 6.0321	221.84 2.4 4.564 0.8820 5.7801

**3.5.1. Langmuir isotherm.** The Langmuir model, based on monolayer coverage,<sup>63</sup> was fitted to experimental data and the parameters and statistical fit quality are given in Table 5;  $q_e$  is the amount of ions sorbed at equilibrium ( $\text{mg g}^{-1}$ ),  $K_L$  is the Langmuir constant related to the energy of biosorption ( $\text{L mg}^{-1}$ ),  $Q_{\max}$  is the maximum sorption capacity corresponding to complete monolayer coverage ( $\text{mg g}^{-1}$ ), and  $C_e$  is the equilibrium solute concentration ( $\text{mg L}^{-1}$ ). A plot of  $C_e/q_e$  versus  $C_e$  should be a straight line with a slope of  $1/Q_{\max}$  and an intercept at  $1/K_L Q_{\max}$ . The dimensionless separator factor ( $R_L$ ) is the essential characteristic of this model, while its value is a reliable indicator for the type of biosorption isotherm. The value of  $R_L$  indicates the shape of the isotherms to be either irreversible ( $R_L = 0$ ), favorable ( $0 < R_L < 1$ ) or unfavorable ( $R_L > 1$ ).

**3.5.2. Freundlich isotherm.** The Freundlich model is an empirical model allowing for multilayer adsorption on adsorbent.<sup>64</sup> The equation and values of the isotherm constants with the correlation coefficients are given in Table 5, where  $K_F$  is the Freundlich constant and  $n$  is the intensity of biosorption. When the value of  $n$  is close to 0, the adsorbent is a heterogeneous surface. Furthermore, if the value of  $n$  ranges between 1 and 10, the biosorption process is thought to be acceptable. When the value of  $n$  is bigger than 1, the physical process occurs naturally. The chemical process takes place when the values of  $n$  is lower than 1.

**3.5.3. Temkin isotherm.** The Temkin isotherm describes the behavior of adsorption systems on heterogeneous surfaces.<sup>65</sup> The modelling of the Temkin equation allowed calculation of its coefficients, which are summarized in Table 5.  $B_1 = RT/b$  ( $\text{J mol}^{-1}$ ) and is the Temkin constant related to heat of sorption,  $R$  is the gas constant ( $8.314 \text{ J mol}^{-1} \text{ K}^{-1}$ ),  $T$  ( $\text{K}$ ) is the absolute temperature, and  $B_1$  and  $K_T$  ( $\text{L g}^{-1}$ ) are the Temkin isotherm constants.

**3.5.4. Dubinin-Radushkevich isotherm.** The Dubinin and Radushkevich (D-R) model was chosen to calculate the apparent free energy of biosorption.<sup>66</sup> The linear form of the D-R isotherm equation and parameter constants (Table 5) are based on the following parameters:  $q_e$  is the amount of bio-sorbed analytes on the biomass ( $\text{mol g}^{-1}$ );  $q_s$  is the maximum biosorption capacity ( $\text{mol g}^{-1}$ );  $\beta$  is the activity coefficient ( $\text{mol}^2 \text{ J}^{-2}$ ) corresponding to mean energy of biosorption; and  $\varepsilon$  is the Polanyi potential which is calculated through eqn (8)

$$\varepsilon = RT \ln \left( 1 + \frac{1}{C_e} \right) \quad (8)$$

where  $R$  is the gas constant ( $8.314 \text{ J mol}^{-1} \text{ K}^{-1}$ ) and  $T$  ( $\text{K}$ ) is the absolute temperature. Using the activity coefficient, it is possible to estimate the mean energy of biosorption ( $\text{kJ mol}^{-1}$ ), which represents an indication of the mechanism involved in the biosorption (Table 5). The biosorption process is chemically controlled when the  $E$  value falls in the range 8 to 16  $\text{kJ mol}^{-1}$ , while the physical mechanism is the main force at  $E$  values lower than 8  $\text{kJ mol}^{-1}$ .

The results for the linear coefficients of determination ( $R^2$ ) and non-linear chi-square tests ( $\chi^2$ ) for all biosorption isotherms (Table 5) show that smaller  $\chi^2$  and higher  $R^2$  values simultaneously support the superiority of the Langmuir model

for best representation of the experimental data over the whole concentration range. The maximum biosorption capacity of the yeast biomass according to the Langmuir isotherm model was 31.96, 24.40 and 25.77  $\text{mg g}^{-1}$  for  $\text{Zn}^{2+}$ ,  $\text{Ni}^{2+}$  and  $\text{Co}^{2+}$  ions, respectively. The magnitudes of  $R_L$  for the biosorption process studied at different initial ions concentrations changed in the range of 0 and 1 and confirm favorable sorption of  $\text{Zn}^{2+}$ ,  $\text{Ni}^{2+}$  and  $\text{Co}^{2+}$  ions onto the yeast. The value of the Freundlich constants,  $n$ , for all ions  $\text{Zn}^{2+}$ ,  $\text{Ni}^{2+}$  and  $\text{Co}^{2+}$  are greater than 1 and lie in the range of 2–10 indicating more favorable biosorption. The  $n$  values for metal ions were between 4.548 and 5.160 suggesting their favorable biosorption onto the yeast biomass. The values of the calculated mean energy ( $E$ ) of biosorption for the metal ions were less than 8  $\text{kJ mol}^{-1}$  and confirm the high contribution of physical force on the biosorption efficiency.

### 3.6. Kinetic models

The pseudo-first-order,<sup>67</sup> second order,<sup>68</sup> intraparticle diffusion<sup>69</sup> and Elovich<sup>70</sup> kinetic models were used in this work. The

**Table 6** Kinetic parameters for the biosorption of ions onto *Yarrowia lipolytica* ISF7 in the single component system

Model	$\text{Zn}^{2+}$ (30 $\text{mg L}^{-1}$ )	$\text{Ni}^{2+}$ (25 $\text{mg L}^{-1}$ )	$\text{Co}^{2+}$ (30 $\text{mg L}^{-1}$ )
<b>Pseudo-first-order-kinetics</b>			
Equation: $\log(q_e - q_t) = \log(q_e) - k_1 t / 2.3037$			
Plot: $\log(q_e - q_t)$ vs. $t$			
$k_1$ ( $\text{min}^{-1}$ )	0.1163	0.0796	0.0804
$q_e$ (calc) ( $\text{mg g}^{-1}$ )	11.428	5.442	6.994
$R^2$	0.9692	0.9583	0.9051
$\chi^2$	0.8970	2.5760	3.4531
<b>Pseudo-second-order-kinetics</b>			
Equation: $(t/q_t) = 1/(k_2 q_e^2) + 1/q_e(t)$			
Plot: $(t/q_t)$ vs. $t$			
$k_2$ ( $\text{min}^{-1}$ )	0.0092	0.0274	0.0197
$q_e$ (calc) ( $\text{mg g}^{-1}$ )	19.120	14.663	17.667
$R^2$	0.9977	0.9989	0.9998
$\chi^2$	0.0063	0.0112	0.0235
<b>Intraparticle diffusion</b>			
Equation: $q_t = K_{\text{dif}} t^{1/2} + C$			
Plot: $q_t$ vs. $t^{1/2}$			
$K_{\text{dif}}$ ( $\text{mg g}^{-1} \text{ min}^{-1/2}$ )	1.516	0.8824	0.8666
$C$ ( $\text{mg g}^{-1}$ )	7.347	8.492	11.085
$R^2$	0.9109	0.9353	0.9462
$\chi^2$	3.7504	3.4310	2.8731
<b>Elovich</b>			
Equation: $q_t = 1/\beta \ln(\alpha\beta) + 1/\beta \ln(t)$			
Plot: $q_t$ vs. $\ln(t)$			
$\beta$ ( $\text{mg g}^{-1} \text{ min}^{-1}$ )	0.2927	0.7092	0.5192
$\alpha$ ( $\text{g mg}^{-1}$ )	19.544	24.658	30.450
$R^2$	0.9655	0.9771	0.9762
$\chi^2$	0.4751	0.3202	0.3643
<b>Experimental data</b>			
$q_e$ (exp) ( $\text{mg g}^{-1}$ )	18.925	14.018	16.758

equations presented in Table 6 were used for interpretation and explanation of experimental data.

The pseudo-second order gave a good fit to the biosorption data ( $R^2 = 0.999$  for  $Zn^{2+}$ ,  $Ni^{2+}$  and  $Co^{2+}$  ions). According to the correlation coefficients, the kinetic models reveal that the pseudo-second order with its high correlation coefficients ( $Zn^{2+}$ : 0.9977,  $Ni^{2+}$ : 0.9989 and  $Co^{2+}$ : 0.9998) and lower  $\chi^2$  values ( $Zn^{2+}$ : 0.0063,  $Ni^{2+}$ : 0.0112 and  $Co^{2+}$ : 0.0235) has a better ability to represent the fitting model for the kinetics of  $Zn^{2+}$ ,  $Ni^{2+}$  and  $Co^{2+}$  ions onto *Yarrowia lipolytica* ISF7. The  $q_{e(\text{exp})}$  values of 18.925 for  $Zn^{2+}$ , 14.018 for  $Ni^{2+}$ , and 6.758 mg g<sup>-1</sup> for  $Co^{2+}$  were in close agreement with  $q_{e(\text{calc})}$  (19.120 for  $Zn^{2+}$ ; 14.663 for  $Ni^{2+}$ ; 17.667 mg g<sup>-1</sup> for  $Co^{2+}$ ) for the pseudo-second order model.

The Weber–Morris intraparticle diffusion model gives idea about mass transfer resistance corresponding to biosorption of  $Zn^{2+}$ ,  $Ni^{2+}$  and  $Co^{2+}$  ions. The  $R^2$  values for this diffusion model were 0.9109, 0.9353 and 0.9462 for  $Zn^{2+}$ ,  $Ni^{2+}$  and  $Co^{2+}$  ions. This result indicates that the biosorption of ions onto *Yarrowia lipolytica* ISF7 follows an intraparticle diffusion model. The Elovich rate equation uses constants for biosorption and desorption to describe the kinetics of chemisorption on highly heterogeneous surfaces. The results obtained by applying this model reveal the presence of acceptable correlation coefficients ( $R^2$  of 0.9655 for the  $Zn^{2+}$  ion biosorption of  $Zn^{2+}$ ).

### 3.7. FTIR and scanning electron microscopy/energy dispersed analysis of X-rays (SEM/EDAX)

The functional groups involved in metal ion biosorption were studied by FTIR spectra (Fig. 4) before and after metal ion biosorption. There was a change in the intensity of the bands in

the FTIR spectra of the yeast biomass after binding with the  $Zn^{2+}$ ,  $Ni^{2+}$  and  $Co^{2+}$  ions.

Fig. 4 shows the presence of broad and strong bands at 3000–3600 cm<sup>-1</sup> corresponding to hydroxyl groups (–OH). The peaks at 1500–1750 cm<sup>-1</sup> are related to C=C stretches of aromatic rings, while the peaks at 900–1125 cm<sup>-1</sup> are assigned to the C–O stretching of alcohols and carboxylic acids. The peaks observed at 1250–1500 cm<sup>-1</sup> are assigned to C–H groups. The results indicate that the functional groups mentioned above are mainly involved in the biosorption of the studied metal ions. In addition, the frequency change observed in the functional groups of the biomass after metal ion biosorption show a high contribution of biomass functional groups on biosorption process efficiency. The asymmetric stretching vibration of N–H was shifted from 1540.85 to 1535.06 cm<sup>-1</sup>. The stretching vibration of  $\delta\text{CH}_2 + \delta\text{OCH} + \delta\text{CCH}$  group was shifted from 1400 to 1390.43 cm<sup>-1</sup> in the yeast. The band shift from 1234.2 to 1390.43 cm<sup>-1</sup> was assigned to  $\delta\text{CCH} + \delta\text{OCH}$  group involvement. The strong C–O band is due to alcohol primary  $-\text{CH}_2\text{OH}$  shifting 1072 from 1076 cm<sup>-1</sup>. The band shift from 879.36 to 887.10 cm<sup>-1</sup> was assigned to N–H group involvement.

The FTIR spectra corresponding to the biosorption of metal ions onto the biomass revealed the involvement of hydroxyl, carboxyl, carbonyl and amino groups which supply suitable sites for complexation,<sup>40,71,72</sup> assuming that coordination bonds are formed between metal ions and the functional groups (amino and carboxyl groups) of cell walls which account for the biosorption of  $Zn^{2+}$ ,  $Ni^{2+}$  and  $Co^{2+}$  ions onto *Yarrowia lipolytica* ISF7.<sup>41</sup> The shifts of the peaks to new values of 1390.43, 1535.06, 1054.87 and 887.10 cm<sup>-1</sup> after metal ion biosorption (Fig. 4)

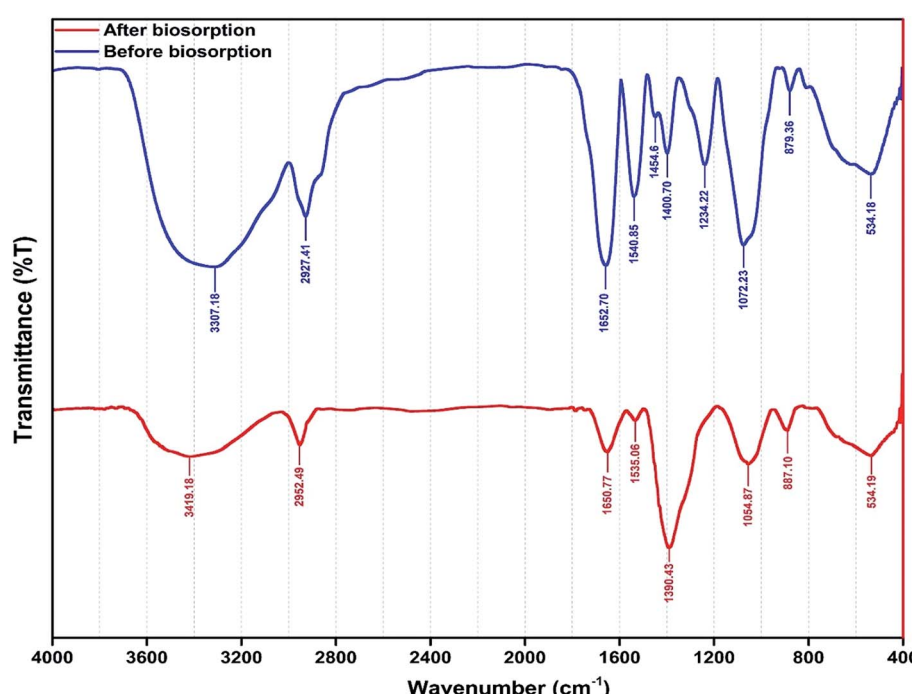


Fig. 4 FTIR spectra of *Yarrowia lipolytica* ISF7 (a) before biosorption and (b) after biosorption.

confirm the interaction between the corresponding functional groups and metal ions.

The SEM images of the incubated *Yarrowia lipolytica* ISF7 cells (Fig. 5a) at a magnification of 5000 $\times$  show the presence of characteristic budding oval yeast cells.

The EDAX analysis conclusively identified them as: Ca, Al, Si, Na, P, S, Cl, K, Ti and Fe with no signal corresponding to Zn<sup>2+</sup>, Ni<sup>2+</sup> and Co<sup>2+</sup> (see Fig. 5a). The yeast contains both inorganic and organic matter, mainly in the forms of iron, alumina, silica and carbonates. The EDAX spectrum of these nodules shows the presence of Zn<sup>2+</sup>, Ni<sup>2+</sup> and Co<sup>2+</sup> signals and other elemental signals (Fig. 5b) consistent with the uptake isotherm. The analysis results confirm the biosorption of Zn<sup>2+</sup>, Ni<sup>2+</sup> and Co<sup>2+</sup> by *Yarrowia lipolytica* ISF7, and that the ions are mainly located superficially in the biosorbent structure.

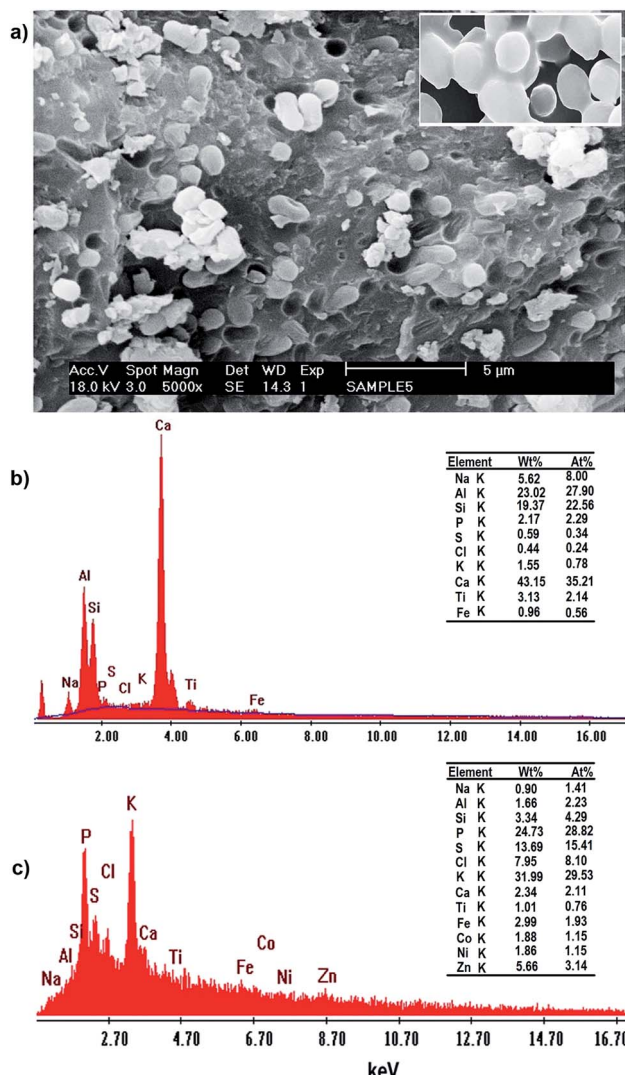


Fig. 5 (a) SEM micrographs and EDAX spectra of *Yarrowia lipolytica* ISF7: (b) in the absence of metal ions and (c) after metal ion biosorption ( $C_0 = 20 \text{ mg L}^{-1}$ ).

Table 7 Comparison of the biosorption of ions by different methods and adsorbents

Adsorbent	Sorption capacity (mg g <sup>-1</sup> )			pH	Ref.
	Zn <sup>2+</sup>	Ni <sup>2+</sup>	Co <sup>2+</sup>		
<i>Aspergillus niger</i>	—	6.80	—	6.0	26
<i>Saccharum bengalense</i>	—	15.79	—	5.0	28
<i>M. hiemalis</i>	—	15.83	—	8.0	73
<i>Aspergillus niger</i>	—	4.82	—	6.3	11
<i>Saccharum bengalense</i>	—	—	1.7	6.5	29
Brown algae	1.42	1.13	—	6.0	30
Baker's yeast	—	11.40	—	6.8	10
Cross-linked metal-imprinted chitosans with epichlorohydrin	14.74	29.23	—	5.0	31
<i>Aspergillus niger</i>	22.62	—	19.881	5.0	27
<i>Chrysanthemum indicum</i>	—	—	14.84	5.0	16
Brown algae <i>C. indica</i>	—	—	54.640	5.0	19
<i>Jania rubens</i>	—	—	32.600	5.0	17
<i>Sophora japonica</i> pod powder	25.71	30.3	—	6.0–7.0	32
Coconut shell	1.56	3.68	—	6.0	74
<i>Sargassum glaucescens</i> nanoparticles	—	28.73	10.11	6.0	33
<i>Aspergillus awamori</i>	—	7.13	—	5.0	75
<i>Mucor hiemalis</i>	—	13.60	—	8.0	76
<i>Hizikia fusiformis</i>	10.56	13.90	—	4.0–6.0	34
<i>Myriophyllum spicatum</i> L.	3.00	6.80	—	5.0	77
Activated sludge	7.78	15.69	—	5.0–6.0	78
Lime stone	0.038	0.012	—	4.0–6.0	9
Lignin	5.99	11.25	—	4.8	79
<i>Geobacillus toebii</i> sub sp. <i>decanicus</i>	29.0	42.0	—	4.0–5.0	21
<i>Geobacillus thermoleovorans</i> sub sp. <i>stromboliensis</i>	21.1	21	—	4.0–5.0	21
<i>Rhizopus oryzae</i> (bread mold)	—	—	13.56	7.0	18
<i>Saccharomyces cerevisiae</i>	16.94	—	21.52	4.0–6.0	35
<i>Yarrowia lipolytica</i> ISF7	31.96	24.40	25.77	6.0	This work

### 3.8. Comparison with other biosorbents

The maximum sorption capacities ( $Q_{\max}$ ) of Zn<sup>2+</sup>, Ni<sup>2+</sup> and Co<sup>2+</sup> ions on various biosorbents in the literature are listed in Table 7. The sorption capacity increased when the initial concentration of the metals increased. It is seen that the sorption capacity of the yeast is higher than that of other biosorbents. Hence, it can be concluded that yeast could be employed as effective low-

cost adsorbent for biosorption of  $Zn^{2+}$ ,  $Ni^{2+}$  and  $Co^{2+}$  ions from aqueous solution.

## 4. Conclusion

The use of an experimental design allowed the rapid screening of a large experimental domain for optimization of the  $Zn^{2+}$ ,  $Ni^{2+}$  and  $Co^{2+}$  removal efficiency of *Yarrowia lipolytica* ISF7. Using a central composite design, quadratic and interaction terms were revealed and the location of the optimum set of experimental conditions was determined. The *P* and *F*-values and model adequacy were tested through lack-of-fit (LOF) and verified successfully by the validation of experimental data. The multiple correlation coefficient of determination ( $R^2$ ) was found to be 0.9919 for  $Zn^{2+}$ , 0.9942 for  $Ni^{2+}$  and 0.9941 for  $Co^{2+}$  which suggests that the actual data fitted well with the predicted data. The equilibrium biosorption data are correlated with Langmuir, Freundlich, Temkin and D-R isotherm equations. The statistical parameters indicate that the Langmuir equation is the best fit. The maximum monolayer biosorption capacities for  $Zn^{2+}$ ,  $Ni^{2+}$  and  $Co^{2+}$  are found to be 31.96, 24.40 and 25.77  $mg\ g^{-1}$  respectively. The kinetic study indicates that the rate of biosorption conforms to the Lagergren rate equation. FTIR studies revealed the possible involvement of hydroxyl and carboxyl groups in  $Zn^{2+}$ ,  $Ni^{2+}$  and  $Co^{2+}$  biosorption. FTIR and SEM-EDAX analyses also suggested a possible coordination between heavy metals and the functional groups on the yeast surfaces.

## Acknowledgements

The authors thank the Research Council of the Yasouj University and Iran National Science Foundation for financially supporting this work.

## References

- 1 A. H. Sulaymon, S. E. Ebrahim and M. J. Mohammed-Ridha, *Environ. Sci. Pollut. Res. Int.*, 2013, **20**, 175–187.
- 2 M. M. Areco, S. Hanela, J. Duran and S. Afonso Mdos, *J. Hazard. Mater.*, 2012, **213–214**, 123–132.
- 3 S. Hajati, M. Ghaedi and S. Yaghoubi, *J. Ind. Eng. Chem.*, 2015, **21**, 760–767.
- 4 J. Sun, Z. Liu, Y. Wang, S. Xiao, M. Pei, X. Zhao and G. Zhang, *RSC Adv.*, 2015, **5**, 100873–100878.
- 5 Y. Shuhong, Z. Meiping, Y. Hong, W. Han, X. Shan, L. Yan and W. Jihui, *Carbohydr. Polym.*, 2014, **101**, 50–56.
- 6 T. Liu, Y. Dong, X. Wan, W. Li and Y. Yao, *RSC Adv.*, 2015, **5**, 76939–76942.
- 7 R. Shen, D. Liu, C. Hou, J. Cheng and D. Bai, *Anal. Methods*, 2016, **8**, 83–88.
- 8 S. B. Khan, M. M. Rahman, H. M. Marwani, A. M. Asiri and K. A. Alamry, *J. Taiwan Inst. Chem. Eng.*, 2014, **45**, 2770–2776.
- 9 H. A. Aziz, M. N. Adlan and K. S. Ariffin, *Bioresour. Technol.*, 2008, **99**, 1578–1583.
- 10 V. Padmavathy, P. Vasudevan and S. C. Dhingra, *Process Biochem.*, 2003, **38**, 1389–1395.
- 11 D. H. K. Reddy, K. Seshaiyah, A. V. R. Reddy and S. M. Lee, *Carbohydr. Polym.*, 2012, **88**, 1077–1086.
- 12 X. C. Song, Y. F. Zheng, H. Y. Yin, J. N. Liu and X. D. Ruan, *New J. Chem.*, 2016, **40**, 130–135.
- 13 T. Itakura, S. Horike, M. Inukai and S. Kitagawa, *Dalton Trans.*, 2016, DOI: 10.1039/c5dt03286e.
- 14 R. Alam, T. Mistri, R. Bhowmick, A. Katarkar, K. Chaudhuri and M. Ali, *RSC Adv.*, 2016, **6**, 1268–1278.
- 15 S. B. Khan, A. M. Asiri, M. M. Rahman, H. M. Marwani and K. A. Alamry, *Phys. E*, 2015, **70**, 203–209.
- 16 S. Vilvanathan and S. Shanthakumar, *Process Saf. Environ. Prot.*, 2015, **96**, 98–110.
- 17 W. M. Ibrahim, *J. Hazard. Mater.*, 2011, **192**, 1827–1835.
- 18 M. Gharieb, A. Al-Fakih and M. Ali, *Arabian J. Sci. Eng.*, 2014, **39**, 2435–2446.
- 19 M. Akbari, A. Hallajisani, A. R. Keshtkar, H. Shahbeig and S. Ali Ghorbanian, *J. Environ. Chem. Eng.*, 2015, **3**, 140–149.
- 20 N. R. Shinde, A. V. Bankar, A. R. Kumar and S. S. Zinjarde, *J. Environ. Manage.*, 2012, **102**, 115–124.
- 21 S. Özdemir, E. Kilinc, A. Poli, B. Nicolaus and K. Güven, *Chem. Eng. J.*, 2009, **152**, 195–206.
- 22 S. B. Khan, K. A. Alamry, H. M. Marwani, A. M. Asiri and M. M. Rahman, *Composites, Part B*, 2013, **50**, 253–258.
- 23 S. Y. Kim, M. R. Jin, C. H. Chung, Y. S. Yun, K. Y. Jahng and K. Y. Yu, *J. Biosci. Bioeng.*, 2015, **119**, 433–439.
- 24 M. Ghaedi, S. Hajati, B. Barazesh, F. Karimi and G. Ghezelbash, *J. Ind. Eng. Chem.*, 2013, **19**, 227–233.
- 25 M. M. Rahman, S. B. Khan, H. M. Marwani and A. M. Asiri, *Superlattices Microstruct.*, 2014, **71**, 93–104.
- 26 M. Amini, H. Younesi and N. Bahramifar, *Chemosphere*, 2009, **75**, 1483–1491.
- 27 Z. Hajahmadli, H. Younesi, N. Bahramifar, H. Khakpour and K. Pirzadeh, *Water Resourc. Ind.*, 2015, **11**, 71–80.
- 28 M. I. Din and M. L. Mirza, *Int. J. Biol. Macromol.*, 2013, **54**, 99–108.
- 29 M. Imran Din, M. L. Mirza, S. Ata, M. Athar and I. U. Mohsin, *J. Chem.*, 2012, **2013**, 1–11.
- 30 Y. Liu, Q. Cao, F. Luo and J. Chen, *J. Hazard. Mater.*, 2009, **163**, 931–938.
- 31 C. Y. Chen, C. Y. Yang and A. H. Chen, *J. Environ. Manag.*, 2011, **92**, 796–802.
- 32 M. Amer, R. Ahmad and A. Awwad, *Int. J. Ind. Chem.*, 2015, **6**, 67–75.
- 33 A. Esmaeili and A. Aghababai Beni, *Int. J. Environ. Sci. Technol.*, 2015, **12**, 2055–2064.
- 34 W.-S. Shin and Y.-K. Kim, *Environ. Earth Sci.*, 2014, **71**, 4107–4114.
- 35 S. Farhan and A. Khadom, *Int. J. Ind. Chem.*, 2015, **6**, 119–130.
- 36 S. Zinjarde, M. Apte, P. Mohite and A. R. Kumar, *Biotechnol. Adv.*, 2014, **32**, 920–933.
- 37 M. Jain, S. Zinjarde, D. Deobagkar and D. Deobagkar, *Mar. Pollut. Bull.*, 2004, **49**, 783–788.
- 38 R. Lanciotti, A. Gianotti, D. Baldi, R. Angrisani, G. Suzzi, D. Mastrocoda and M. Guerzoni, *Bioresour. Technol.*, 2005, **96**, 317–322.
- 39 S. Papanikolaou, I. Chevalot, M. Komaitis, I. Marc and G. Aggelis, *Appl. Microbiol. Biotechnol.*, 2002, **58**, 308–312.

40 N. R. Shinde, A. V. Bankar, A. R. Kumar and S. S. Zinjarde, *J. Environ. Manag.*, 2012, **102**, 115–124.

41 A. V. Bankar, A. R. Kumar and S. S. Zinjarde, *J. Hazard. Mater.*, 2009, **170**, 487–494.

42 S. García, M. Prado, R. Dégano and A. Domínguez, *J. Biological Chem.*, 2002, **277**, 37359–37368.

43 P. S. Pimprikar, S. S. Joshi, A. R. Kumar, S. S. Zinjarde and S. K. Kulkarni, *Colloids Surf., B*, 2009, **74**, 309–316.

44 C.-Y. Tai, S.-J. Jiang and A. Sahayam, *Food Chem.*, 2016, **192**, 274–279.

45 É. F. Batista, A. dos Santos Augusto and E. R. Pereira-Filho, *Talanta*, 2016, **150**, 206–212.

46 B. Feist and B. Mikula, *Food Chem.*, 2014, **147**, 302–306.

47 M. M. Rahman, S. B. Khan, H. M. Marwani and A. M. Asiri, *PLoS*, 2014, **9**, 4084.

48 V. C. D. Peronico and J. L. Raposo, *Food Chem.*, 2016, **196**, 1287–1292.

49 X. Wen, S. Yang, H. Zhang and Q. Deng, *Microchem. J.*, 2016, **124**, 60–64.

50 G. Luis, C. Rubio, C. Revert, A. Espinosa, D. González-Weller, A. Gutiérrez and A. Hardisson, *J. Food Compos. Anal.*, 2015, **39**, 48–54.

51 X. Zhu, Y. Cui, X. Chang and H. Wang, *Talanta*, 2016, **146**, 358–363.

52 A. Asfaram, M. Ghaedi, A. Goudarzi and M. Rajabi, *Dalton Trans.*, 2015, **44**, 14707–14723.

53 J. Zolgharnein and A. Shahmoradi, *J. Chem. Eng. Data*, 2010, **55**, 3428–3437.

54 A. Asfaram, M. Ghaedi, S. Hajati and A. Goudarzi, *RSC Adv.*, 2015, **5**, 72300–72320.

55 E. A. Dil, M. Ghaedi, A. M. Ghaedi, A. Asfaram, A. Goudarzi, S. Hajati, M. Soylak, S. Agarwal and V. K. Gupta, *J. Ind. Eng. Chem.*, 2016, **34**, 186–197.

56 A. Asfaram, M. Ghaedi, S. Hajati, A. Goudarzi and A. A. Bazrafshan, *Spectrochim. Acta, Part A*, 2015, **145**, 203–212.

57 G. Yan and T. Viraraghavan, *Water Res.*, 2003, **37**, 4486–4496.

58 C. Gao, H. Zhu, M. Zhang, T. Tan, J. Chen and H. Qiu, *Anal. Methods*, 2015, **7**, 8172–8176.

59 D. Bansal and R. Gupta, *Dalton Trans.*, 2016, **45**, 502–507.

60 A. M. Hessels, K. M. Taylor and M. Merkx, *Metallomics*, 2016, **8**, 211–217.

61 F. N. Azad, M. Ghaedi, K. Dashtian, S. Hajati and V. Pezeshkpour, *Ultrason. Sonochem.*, 2016, **31**, 383–393.

62 A. Asfaram, M. Ghaedi, S. Agarwal, I. Tyagi and V. Kumar Gupta, *RSC Adv.*, 2015, **5**, 18438–18450.

63 I. Langmuir, *J. Am. Chem. Soc.*, 1916, **38**, 2221–2295.

64 H. Freundlich, *Z. Phys. Chem.*, 1906, **57**, 385–471.

65 M. Temkin and V. Pyzhev, *Acta Physicochim. URSS*, 1940, **12**, 217–222.

66 A. Elmaci, T. Yonar and N. Ozengin, *Water Environ. Res.*, 2007, **79**, 1000–1005.

67 S. Lagergren, *K. Svenska Vetenskapsakad. Handl.*, 1898, **24**, 1–39.

68 Y.-S. Ho and G. McKay, *Process Biochem.*, 1999, **34**, 451–465.

69 W. J. Weber and J. C. Morris, *J. Sanit. Eng. Div., Am. Soc. Civ. Eng.*, 1963, **89**, 53–61.

70 C.-Y. Chen, C.-Y. Yang and A.-H. Chen, *J. Environ. Manage.*, 2011, **92**, 796–802.

71 N. Ahalya, T. Ramachandra and R. Kanamadi, *Res. J. Chem. Environ.*, 2003, **7**, 71–79.

72 M. Riaz, R. Nadeem, M. A. Hanif, T. M. Ansari and K. U. Rehman, *J. Hazard. Mater.*, 2009, **161**, 88–94.

73 J. P. K. Wong, Y. S. Wong and N. F. Y. Tam, *Bioresour. Technol.*, 2000, **73**, 133–137.

74 F. Sousa, A. Oliveira, S. Moreira, R. Cavalcante, M. Rosa and R. Nascimento, *Quim. Nova*, 2008, **30**, 1153–1157.

75 F. Shahverdi, M. Ahmadi, S. Avazmoghadam and M. A. Faramarzi, *Environ. Prog. Sustainable Energy*, 2015, **34**, 1356–1364.

76 K. A. Shroff and V. K. Vaidya, *Eng. Life Sci.*, 2011, **11**, 588–597.

77 E. Lesage, C. Mundia, D. Rousseau, A. Van de Moortel, G. Du Laing, E. Meers, F. Tack, N. De Pauw and M. Verloo, *Ecol. Chem. Eng. A*, 2007, **30**, 320–325.

78 A. Hammami, F. González, A. Ballester, M. Blázquez and J. Munoz, *J. Environ. Manage.*, 2007, **84**, 419–426.

79 X. Guo, S. Zhang and X.-Q. Shan, *J. Hazard. Mater.*, 2008, **151**, 134–142.